

Chapter 9

Investigation of Transient Regime in Laminar Separation Bubble Formation



Pedro Bruno Pereira Panisset, Omar Elias Horna Pinedo,
and Igor Braga de Paula

Abstract The transient flow regime related with the formation of laminar separation bubbles (LSB) is examined by time-resolved measurements of the velocity field. The investigated scenario aims at studying the flow in multiple stage turbines, where the wake of airfoils in previous compression stages induces periodic variation of turbulence level in the subsequent airfoils. This can lead to periodic removal and formation of LSB. This process is simulated here by exciting controlled disturbances with a vibrating ribbon. Experiments are carried out in a laminar water channel at PUC-Rio. Longitudinal PIV measurements are performed on a flat plate subjected to an adverse pressure gradient. The pressure gradient is set by false walls with adjustable geometry. Suction is applied on the false wall, in order to avoid the boundary layer separation at this surface. Bubble topology and disturbance growth along the streamwise direction are measured during the transient of bubble formation. Results show spatial amplification over a narrow frequency bandwidth. Dominant non-dimensional frequencies ($St = f\delta^*_s/U$) at late stages of bubble formation are in close agreement with those reported in literature. During the transient the intensity of reverse flow is significantly changed, pointing out for possible changes on the stability mechanisms involved on the bubble reattachment.

Keywords Laminar separation bubble · Boundary layer transition · Hydrodynamic stability

9.1 Introduction

The performance of autonomous aircrafts and turbines, operating at low chord-based Reynold numbers (from 10^4 to 10^6), can be highly affected by the presence of laminar separation bubbles (LSB). The laminar separation bubble appears in this context as a combination of long extend of laminar flow over the airfoil surface and adverse pressure gradient. In this scenario, the transition to turbulent flow can occur in the

P. B. Pereira Panisset · O. E. Horna Pinedo · I. B. de Paula (✉)
Department of Mechanical Engineering, Pontifical Catholic University of Rio de Janeiro,
Rua Marques de São Vicente 225, Gavea, RJ 22451-041, Brazil
e-mail: igordepaula@puc-rio.br

© The Author(s), under exclusive license to Springer Nature Switzerland AG 2023
H. F. Meier et al. (eds.), *Advances in Turbulence*, ABCM Series on Mechanical Sciences
and Engineering, https://doi.org/10.1007/978-3-031-25990-6_9

separated boundary layer which further can cause a flow reattachment to the surface. This closed region formed between the separation point and the reattachment is known as LSB and its topology was detailed in the work of Tani (1964).

First works in the field showed that the presence of LSB creates a plateau on the pressure coefficient distribution in airfoils (Tani 1964, Mayle 1991; Gaster 1969). According to Tani (1964), the bubble can be classified as short bubble and long bubble. Short bubbles are more frequently observed near the suction peak of airfoils operating at low and moderate Reynolds numbers (Mayle 1991) and often do not have a strong influence on the airfoil performance. On the other hand, long bubbles can extend for a significant portion of the chord length and hence affect significantly drag and reduce lift. According to Gaster (1969), this type of bubble is very sensitive to flow conditions. Several parameters can affect the phenomenon including Reynolds number, freestream disturbances (turbulence and acoustic disturbance field), pressure gradient, surface roughness, and temperature gradient, among others (Akpolat et al. 2012). According to Swift (2009) and Yarusevych and Kotsonis (2017), combination of these effects can also influence the bubble dynamics. An important aspect related to LSBs is the occurrence at given flow conditions of the so-called “bubble bursting” events, characterized by a rapid switch between short and long bubble (Serna and Lázaro 2015a, b). This “bursting” can significantly affect the performance of airfoils and change its dynamics. Unfortunately, the phenomenon is not well predicted by current models (Serna and Lázaro 2015a, b). For a proper modeling of this problem, it is important to describe the physics underlying the bubble dynamics. Although several advances have been observed during last decades in the description of regimes of quasi-steady bubbles, very little is known about the bubbles in transient regimes (Yarusevych and Kotsonis 2017). Detailed characterization of bubbles in transient regimes can help to elucidate the dynamics of the bubble formation and the bubble “bursting”.

The goal of current work is to shed further light on the description of the phenomenon by studying experimentally the formation of an LSB. To this end, controlled disturbances were introduced in the boundary layer by means of a vibrating ribbon. The disturbance source was located upstream of the separation region. Initially, the fluctuation amplitude was high enough to remove the bubble. The transient regime related with bubble formation was obtained by a sudden reduction in the level of fluctuations. Experiments were performed on a flat plate subjected to an adverse pressure gradient. Measurements were carried out in a low turbulence and close return water channel at PUC-Rio. The amplitude and frequency of disturbances were controlled by a magnetic actuator. Phase-locked planar and time-resolved PIV measurements were used for extraction of ensemble averaged velocity fields in the LSB region. The manuscript reports validate the apparatus and methods adopted by a comparison against benchmarks available in the literature. Thereafter, measurements performed during the transient regime are presented and discussed.

9.2 Experimental Methodology

The experimental campaign was carried out in a low turbulence level and close return water tunnel. With the aid of a frequency inverter ranging 0.1–20 Hz, an axial motor pump allows to achieve streamwise velocities within a range of 0.05–0.5 m/s. The tunnel is equipped with one honeycomb and four meshes to reduce turbulence in the test section. The contraction rate of the tunnel is 4:1 which is a typical value for quiet water tunnel facilities. It is interesting to mention that low turbulence wind tunnels have usually a much higher contraction rate of about 9:1. The measured turbulence level in the test section is estimated in about 0.25% within a bandwidth of 0.1 to 50 Hz, for velocities up to 0.15 m/s.

A flat plate 3000 mm long was inserted in the test section at 600 mm downstream from the test section inlet. The plate is made of transparent polycarbonate. The plate is equipped with a flap for adjustment of the stagnation point on the leading edge. Above the flat plate a false wall was built in order to create a variable pressure gradient on the plate. In the present configuration, the false wall created a convergent, divergent channel over the plate. The angle of divergent wall could be adjusted in order to provide a prescribed constant adverse pressure gradient. The throat height at the vertex of convergent–divergent channel was fixed in 200 mm. On the divergent part suction slots were machined on the false wall in order to avoid separation. Centrifugal pumps Sarlo2000 were used for boundary layer suction. The water was pumped to the tunnel corner downstream from the test section.

Controlled disturbances were created using a vibrating ribbon made of steel. The oscillation of the ribbon was provided by an electrical magnet with a controlled current. The magnet was placed in a sealed case that was flush mounted with the flat plate surface.

Time-resolved velocity fields were measured using a planar PIV system. High sampling frequency was achieved using a double cavity laser LITRON LDY-300, which provides 30 mJ/pulse at 2 kHz, and a Phantom Miro 341, which has a maximum resolution of 1600×2560 pixels and can run at frequencies up to 800 frames per second at the maximum resolution. Illumination and imaging systems were synchronized by a TSI 610036 synchronizer. For present measurements, the sampling frequency was set to 200 Hz. A set of spherical and cylindrical lens was used to create the illumination plan for PIV measurements. Polyamide particle tracers with diameters of about $20 \mu\text{m}$ and density of 1.03 kg/m^3 were used for flow seeding. Routines developed in LabView and MATLAB allowed to control the image acquisition and the PIV processing, respectively.

9.3 Results

The results obtained in this work are divided into two parts. First, the results regarding the quasi-steady bubble regime with the disturbance generator in the flow are presented. The results obtained in this regime are used for validation of measurement set-up and post-processing strategies. For this validation, the results of the separation bubble were compared with some results reported in the literature. After validation, results related with transient regime are reported. In this last regime, the actuator is used to introduce disturbances with high amplitude in the boundary layer, which removes completely the bubble. The disturbance source is then switched off and the transient regime until the bubble shows a quasi-steady behavior is captured.

9.3.1 Quasi-Steady Regime

One of the important parameters for laminar separation bubbles is the level of adverse pressure gradient. The pressure distribution of this work was estimated with the velocity fields measured with the PIV without the presence of the bubble. To this end, a trip was used to force the laminar-turbulent transition of the boundary layer upstream of the separation and remove the bubble. Thus, the free flow velocity fields were measured by moving the camera and the laser beam along the flat plate. The results are shown in Fig. 1 as a function of the pressure coefficient, assuming that the reference pressure is the static pressure at the last measurement station and that the flow is two dimensional. In the same figure, the vertical lines $L_p/\delta_s^* = 40$ e $L_p/\delta_s^* = 103$ indicate, respectively, the start and end positions of the measurement field ($x/\delta_s^* = 0$ and $x/\delta_s^* = 63$ in the speed contours, Fig. 4. The figure clearly shows the change in the pressure distribution on the plate, caused by the separation. In this case, the distribution presents a pressure plateau, typical of laminar separation bubbles, followed by a recovery. According to the work of Pinedo (2018), in the range where we have the bubble, the pressure gradient is approximately linear.

According to Dovgal et al. (1994), the velocity profile of the boundary layer at the separation point can be fitted by a modified hyperbolic tangent function. In Fig. 2, we have the velocity profile and its derivative very close to the separation location (lines $L_p/\delta_s^* \sim 55$). It is possible to observe that the obtained data are well represented by the function proposed by Dovgal et al. (1994). This function is

$$U(y) = \frac{\tanh(a(y-d)) + \tanh(ad)}{1 + \tanh(ad)} + b\sqrt{3}\eta \exp(-1.5\eta^2 + 0.5)$$

where $\eta = y/d$, b is a measure of the magnitude of the reverse flow, d is the dimensionless height of the inflection point, and a is treated like a free parameter. In this work, the height of the inflection point was used to scale y and d ; consequently, the dimensionless height of the inflection was fixed at $d = 1$. In addition to the velocity

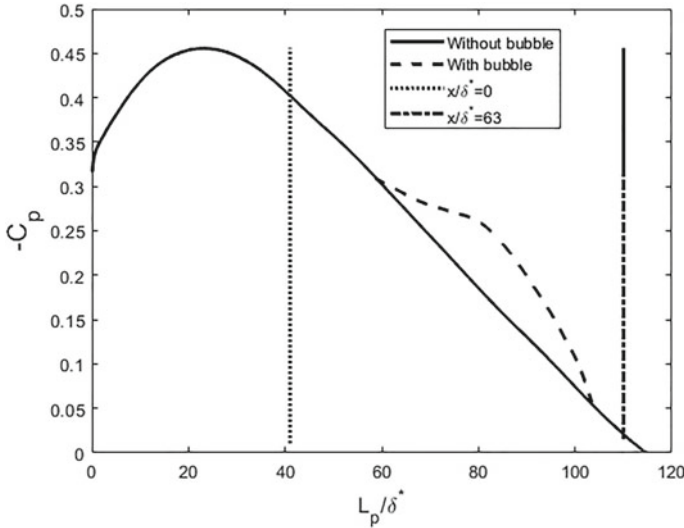
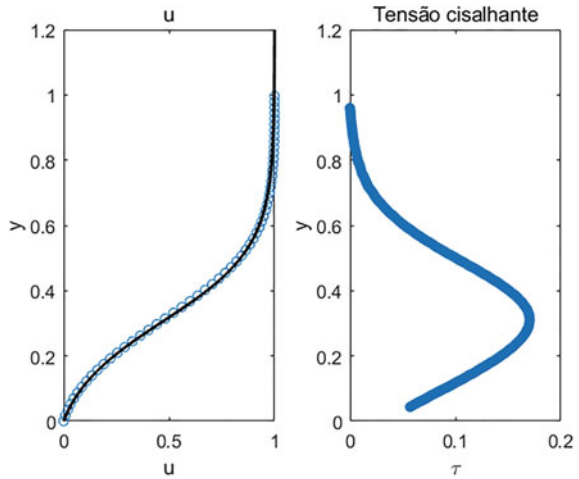


Fig. 1 Pressure distribution with and without the presence of the laminar separation bubble

Fig. 2 Velocity profile $u(y)$ and shear stress $\tau(y)$ at the separation point. Blue circle: experimental data; solid line: modified Dovgal function



profile, the integral parameters of the boundary layer are important to describe the flow characteristics. These parameters are often reported in the literature and can be useful for validation of current results. In Fig. 3, we have the results of the distribution of δ^* , θ , and H measured experimentally. It can be observed that the evolution of the displacement thickness and, consequently, the form factor vary significantly along the flow, in the presence of the separation bubble. The increase in the displacement

thickness and the form factor up to the maximum bubble height, as well as the maintenance of θ , follows the works reported in the literature (Hatman and Wang 1998; Hain et al. 2009).

In the present work, δ_s^* value was 0.0046 and θ_s was 0.0012. Since the study by Tani (1964), Re number values based on the displacement thickness and the momentum thickness at the point of separation ($Re_{\delta_s^*} = u_0 \delta_s^* / \nu$, $Re_{\theta_s} = u_0 \theta_s / \nu$, respectively) have been used as an indicator of the occurrence of the bursting process. In separation bubbles, the bursting process corresponds to its burst and abrupt growth. The respective $Re_{\delta_s^*}$ and Re_{θ_s} values found based on the results obtained with the PIV were 1159 and 302. These values are consistent with the results found in the literature, $350 < Re_{\delta_s^*} < 1305$ and $150 < Re_{\theta_s} < 450$ according to Mayle (1991), Michelis et al. (2017), Serna and Lázaro (2015b).

Figure 4 presents the result for the average velocity field U obtained under constant channel velocity conditions. The average velocity field was calculated by averaging

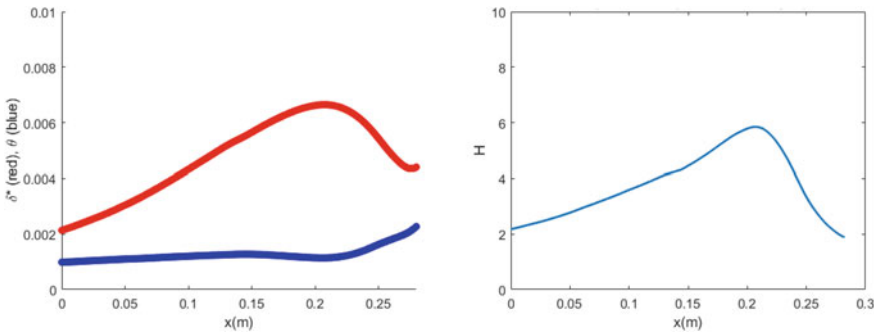
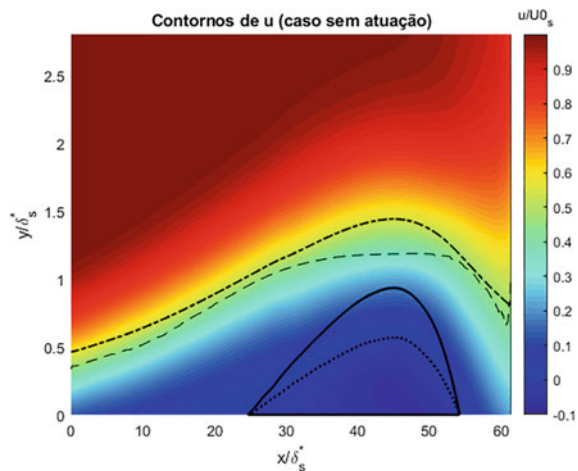


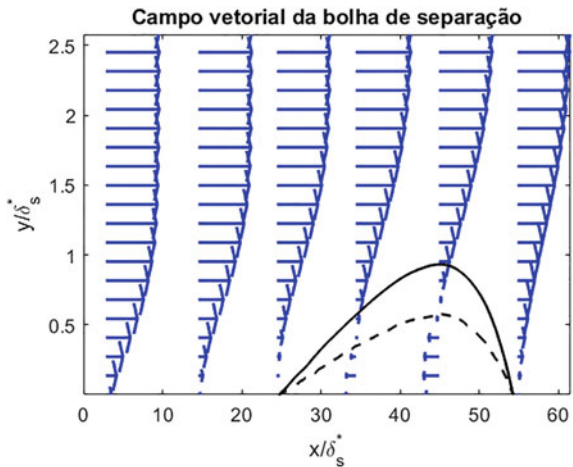
Fig. 3 Boundary layer integral parameters. Left: δ^* (red), θ (blue); Right: shape factor H

Fig. 4 Contour of mean streamwise velocity field U . Dash-dotted line: δ^* , dashed line: inflection points, solid line: stream line $\psi = 0$, dotted line: $U = 0$



6737 instant fields. From this graph, it is possible to identify some characteristic dimensions of the bubble. For this, the streamline ($\psi = 0$) that divides the flow between the inner and outer regions of the bubble is used. It is worth mentioning that the zero velocity line maintains the same points of separation and reattachment of the streamline $\psi = 0$. Based on the results of the streamline, the total bubble length was approximately $L = 140 \text{ mm}$ ($L/\delta_s^* = 29$) and the maximum height was $h = 4.3 \text{ mm}$ ($h/\delta_s^* = 0.94$). Figure 5 show some u velocity profiles along the bubble. It is noticed as a profile close to the laminar profile in positions upstream of the separation. At the separation point, the velocity profile resembles the modified tanh (y)-type profile. Inside the bubble, we can observe the presence of reverse flow and the beginning of the formation of turbulent flow. Didactically, it is possible to separate the bubble length into two regions. The first goes from the separation point to the local of maximum bubble height. This region is called laminar L_I because the flow is still in the initial stages of transition. The second region, in turn, comprises the part that goes from the point of maximum height of the bubble to the reattachment (L_{II}), and is called turbulent due to the fact that the flow has already undergone the transition or is in the final stages of the transition. According to the data, from the experiments, the L_I region has 94 mm ($L_I/\delta_s^* = 20.4$), while the L_{II} region has 42 mm ($L_{II}/\delta_s^* = 8.6$). The relation between (L_I/L_{II}) obtained for the bubble was 2.24 , this value is within the range ($1.6\text{--}3$) reported in the work of Marxen and Henningson (2011). Still on the topological characterization of the bubble, there is the divergence angle (α), another parameter that helps describe the phenomenon. This angle is obtained through the trigonometric relationship between the height (h) of the bubble and the length L_I . Thus, it has to be $\alpha = \tan^{-1}(h/L_I)$. In the present work, the value obtained was $\alpha = 0.046 \text{ rad}$. Finally, the maximum reverse velocity was 6.2% of u_0 . This value is below the threshold for absolute instability proposed in the work of Rodríguez et al. (2013).

Fig. 5 Streamwise velocity profiles along the bubble. Just a few profiles are shown to illustrate the streamwise velocity profiles with the measurement region



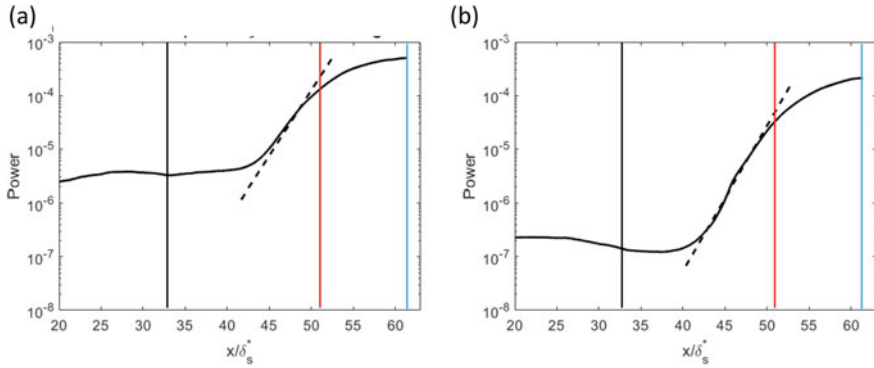


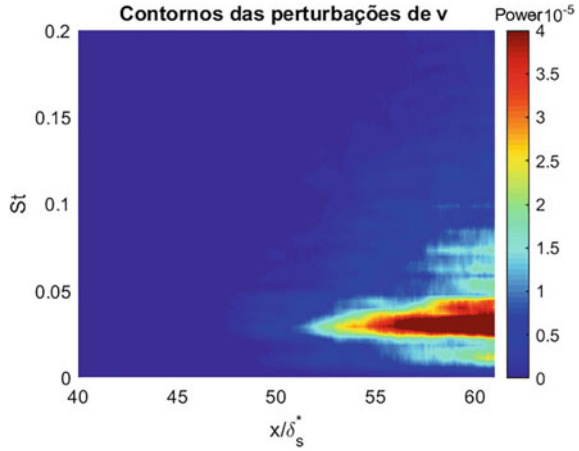
Fig. 6 Growth of the maximum velocity fluctuation (a) u' and (b) v' . Solid thick line: experimental data; dashed line: $St-5/3$; Vertical lines: separation (black), maximum height (red), and reattachment (blue) points

Figure 6a presents the results related to the velocity fluctuations u' distribution. In Fig. 6b, the velocity fluctuations v' are shown. The data in Fig. 6 was obtained along the inflection line in Fig. 4. Unlike the velocity fluctuations u' , the fluctuations of v become relevant only close to the bubble maximum height location ($x/\delta_s^* \sim 45$). Only at the final stages, near the reattachment location, the two components reach values of the same order of magnitude. The growth of these velocity fluctuations corroborate, qualitatively, the results found in several works, for example, in Lengani et al. (2017). According to the figure, disturbances display a nearly exponential amplification (linear in log scale) in a narrow region from $40 < x/\delta_s^* < 50$. Further downstream the disturbances exhibit a saturation and quickly the flow becomes turbulent. In the growth of u' , it is more difficult to visualize exponential behavior because, in this direction, there are small variations in the channel speed that make the signal noisy. Therefore, the analysis of flow fluctuations will focus on the v' component.

Figure 7 shows the contours of the spectral content of the disturbance v' along the flow direction (x). To this end, a Welch's periodogram was applied with a block of 512 points and a 50% overlap between blocks of the time series. The time series for each position (x) was collected at a height (y) corresponding to the inflection line of the base flow velocity profile. According to the figures, the highest energy of fluctuations is concentrated within the bubble reattachment region, where the flow is at final stages of the transition. Within this region the velocity fluctuations show variations of Strouhal number in the interval $0.01 < St < 0.05$. It is interesting to note that a similar range of Strouhal numbers was previously reported in the work of Michelis et al. (2017). In that work, the fluctuations were related with vortex ejection in the reattachment region.

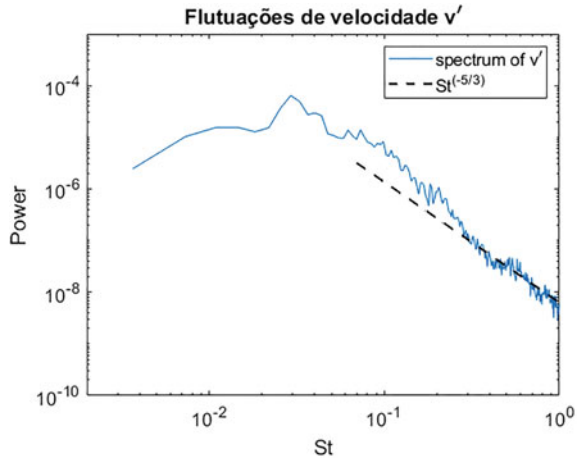
Finally, Fig. 8 presents the power spectrum of v' . A traced line corresponding to Kolmogorov's energy cascade law is also included in the graph as a reference. The velocity fluctuations were obtained at a streamwise location (x) corresponding to the maximum bubble height (x/δ_s^* approx. 45). The spectrum shows higher energy in

Fig. 7 Contours of power spectrum of the velocity fluctuation v' measured at the inflection points of base flow profiles



Strouhal numbers within the interval $0.01 < St < 0.05$. This is the range found in Fig. 7 for stations near and after the reattachment. This suggests a strong relation between most amplified disturbances near the bubble maximum height and those downstream of the reattachment. Indeed, this was previously reported in the work of Michelis et al. (2017), and it is related with generation of vortex in the reattachment region. It is also interesting to note that near the maximum bubble height the high frequencies in the spectrum do already exhibit some adherence with the Kolmogorov cascade ($f^{-5/3}$), even though the flow is not yet turbulent.

Fig. 8 Energy cascade of the wall normal velocity fluctuation v' measured at maximum bubble height



9.3.2 Transient Regime

The transient regime studied in current work covers the regime without boundary layer separation until the complete recovery of the separation bubble. To this end, the disturbance source was activated and suddenly switched OFF. During the period when the source was switched ON, the excitations were tonal with a frequency corresponding to those of most amplified disturbances observed in the quasi-steady regime ($St = 0.05$). The disturbance amplitude was set by adjusting the voltage source to the lowest possible voltage capable of removing the bubble. The bubble elimination was detected visually. After 15 s of actuation and the complete disappearance of the bubble, the system was suddenly turned OFF. A few seconds after the actuator was turned off, the bubble started to grow. This process of recovering the quasi-steady state of the bubble was repeated 30 times, and the results presented in this section represent the average of these 30 acquisitions. A time diagram representing the operation of the equipment during this transient period is illustrated in Fig. 9. The results shown in this section refer to that transient period until the bubble recovers.

Figure 10 shows the mean streamwise velocity fields, obtained with an average of 30 instants of time, for the initial (10a) and final (10b) instants of the transient regime. At first the flow does not present separation boundary layer and therefore there is no reverse flow. It is observed that after the transient, the bubble resembles the one found for the quasi-steady regime (see Fig. 4). The parameters related to the topology of the bubble that were obtained after its recovery are: $L = 140$ mm (L_1/δ_s^*

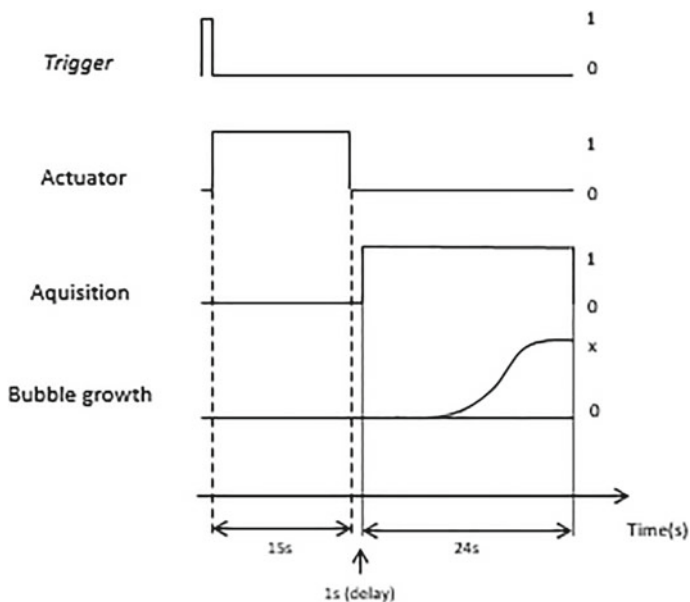


Fig. 9 Time diagram of the transient process data acquisition

= 30.4), $h = 4.2$ mm ($h/\delta_s^* = 0.91$), $L_I = 98$ mm ($L_I/\delta_s^* = 21.3$), $L_{II} = 42$ mm ($L_{II}/\delta_s^* = 9.1$), $\alpha = 0.043$, $L_I/L_{II} = 2.33$, $Re_{\delta_s^*} = 1333$, $Re_{\theta_s} = 310$, and maximum reverse speed was 6.7%. Comparing these results with the case without disturbance actuation, it can be observed that such parameters are, in fact, similar and suggest full bubble recovery. Table 1 shows the summary comparative results between the transient case and the case without disturbing.

Velocity fluctuations were analyzed after its apparent recovery. The idea is to observe whether there is any apparent hysteresis in the bubble shortly after the transient. Figure 11a, b shows the amplification of streamwise and wall normal disturbances, respectively. Fluctuations exhibit a strong amplification close to maximum bubble height. This data was captured at y-position equal to the height of the inflection line. It is possible to identify an exponential growth of these disturbances at stations between $42 < x/\delta_s^* < 50$. The amplification of the disturbances measured without any forcing is in qualitative agreement with those measured after the bubble recovery in the transient regime. For a fair comparison, one should consider that these experiments have to be carried out in different days due to the long time required for

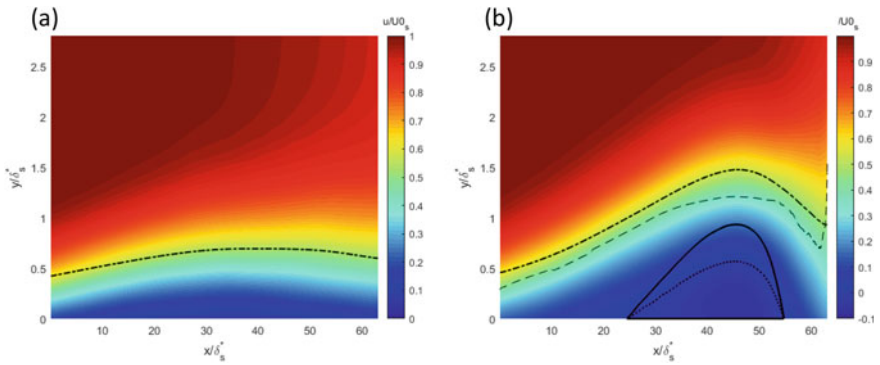


Fig. 10 Contours of mean streamwise velocity field at the beginning (a) and ending (b) of the transient process. Dash-dotted line: δ^* , dashed line: inflection point, solid line: streamline $\psi = 0$, dotted line: $U = 0$

Table 1 Summary comparison of some parameter at the end of the transient and the quasi-steady state of the LSB

Parameters	End of transient	Quasi-steady state
L(mm)	140	136
h(mm)	4.2	4.3
L_I/L_{II}	2.33	2.24
α (rad)	0.043	0.046
L_I/θ_{θ_s}	82	80
Re_{θ_s}	310	302
$Re_{\delta_s^*}$	1333	1159
St_{θ_s}	0.01–0.05	0.01–0.05

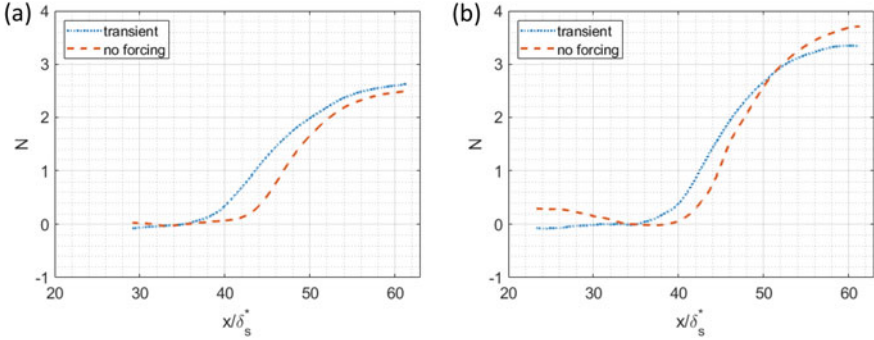


Fig. 11 N-factor of the maximum velocity fluctuations growth (a) u' and (b) v' . Blue dotted line: final instant of transient regime, light brown line: quasi-steady state

each campaign with 30 ensembles. Results suggest that the averaged bubble parameters were in close agreement. However, the growth of disturbances in the transient regime seems to be amplified slightly upstream in comparison to the case without excitation of disturbances. This might be related with residual disturbances near the wall which can remain in the flow for a long time. However, this conjecture demands further investigations.

The evolution of some bubble parameters during the transient period was also analyzed. The analysis includes bubble contour, shape factor H , separation angle (α), and separation and reattachment points. Figure 12a depicts bubble contours, corresponding to the streamline $\psi = 0$, during the transient. According to Michelis et al. (2017), at a certain instant during the transient, the bubble is extended beyond its quasi-steady length in quasi-steady regime. Here this was observed approximately at 12.8 s after the disturbance was switched off. Michelis et al. (2017) highlight some aspects of the phenomenon resemble those of bubble bursting process. It is interesting to note in Fig. 12a that despite the bubble parameters, such as length, height, and separation angle apparently undergo significant variations during the transient, the bubble shape appears to follow a regular pattern. In order to assess the general behavior of the phenomenon during this transient, the bubble dimensions are normalized by its instantaneous separation point (x_s), length (L), and the (h). Contours of normalized bubbles are illustrated in Fig. 12b. It is observed that in beginning of bubble formation the shape is different. However, after 3 s the overall bubble shape is not significantly affected during the transient, even though it exhibits significant changes on its parameters. Most remarkable differences are observed in the region of reattachment.

In Fig. 13a, the shape factor evolution is shown for different instants of time. The maximum in shape factor distributions present remarkable changes in the x -direction at the initial stages due to the fast bubble expansion. As the bubble approaches the quasi-steady topology, the shape factor tends to higher values. This is also in agreement with observations reported by Yarusevych and Kotsonis (2017). For a better comparison of the shape factors at the different instants, it was decided to subtract the

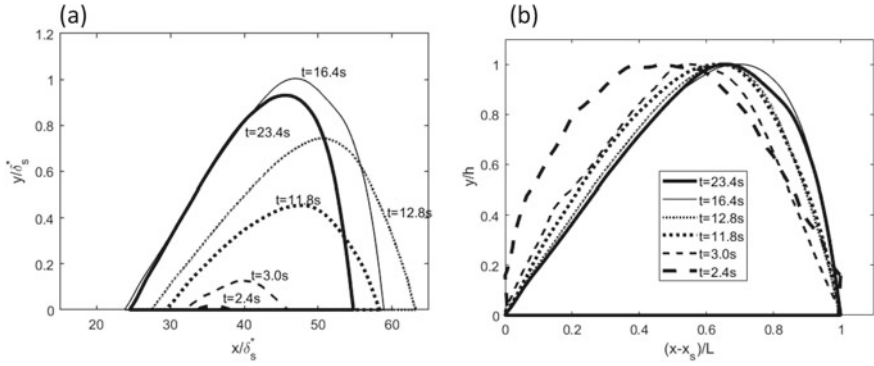


Fig. 12 Bubble streamline $\psi = 0$ for different time instants. **a** Non-normalized contour and **b** Normalized contour

position corresponding to the separation point x_s from the x -coordinates. Thus, the shape factor distributions of Fig. 13b are referenced to the separation point instead of a fixed reference. It is observed that the separation point in the transient regime occurs for a condition of H practically constant. This suggests that boundary layer separation is mostly dependent on local integral parameters. Therefore, separation criteria based on momentum thickness might be applicable also to transient regimes.

Figure 14 shows the transient locations of separation and reattachment points and also the position of maximum bubble heights. At the instant $t = 2$ s, there is the first identification of the boundary layer separation. From this time on, the bubble begins to grow until it stabilizes with characteristics similar to those of quasi-steady regime. At instants in the interval $2 < t < 5$ s, it is observed that the separation point moves continuously upstream, while x_h and x_r float around a single position. For times between 5 and 10 s, the bubble seems to assume a laminar length (L_I) very similar to the turbulent length (L_{II}). Near $t = 11.8$ s a sudden jump on the positions can be seen. This behavior can be linked to the ejection of a large vortex or to a discontinuity

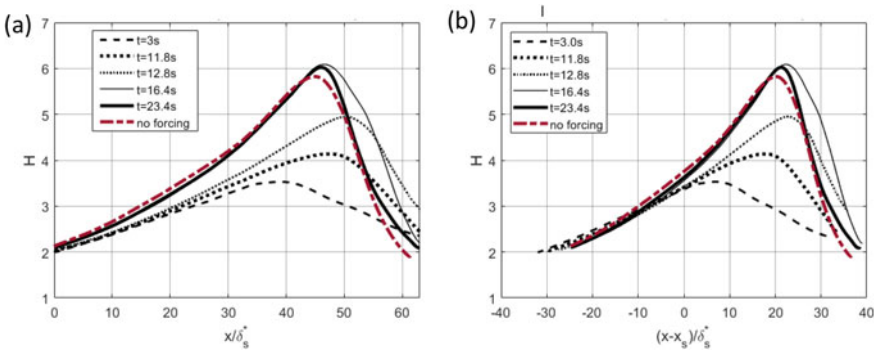
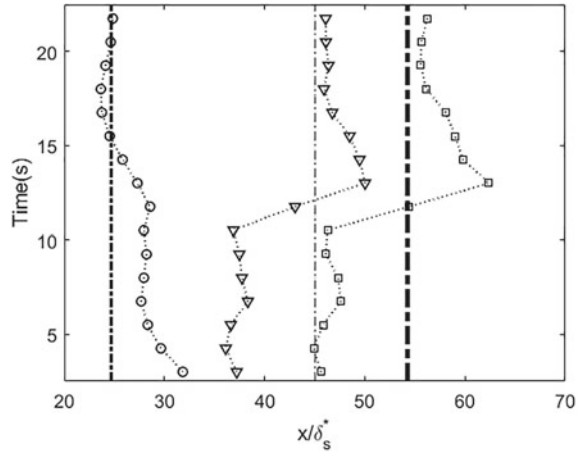


Fig. 13 Shape factor H at the transient regime. **a** Non-normalized H , **b** Normalized H

Fig. 14 Separation (circle), maximum height (triangle), and reattachment (square) points of the bubble at the transient process in the x-direction. Dashed-dotted line: separation, maximum height, and reattachment points, respectively, at the quasi-steady state



in the sampling of the phenomenon due to the acquisition of two data series at two different moments. Due to the time needed for the bubble to recover, the acquisition of the transient regime had to be divided into two parts. In the first part, the instants $t_1 = 0$ to $t_{N/2} = 11.8$ s were measured; and in the second, the instants $t_{N/2+1} = 11.8$ s to $t_N = 24$ s. However, these measurements were made at a 1-day interval. Due to the high sensitivity of the bubble, some small change in the flow conditions in the channel may have occurred, causing a discontinuity of the data. Anyway, this does not refute the results presented so far, since their validation demonstrates that the recovered bubble has characteristics similar to the undisturbed case. Therefore, the variation may have caused some loss of information about the bubble evolution in the transient regime. However, it is still possible to identify the maximum bubble elongation near $t = 12.7$ s. From this moment, the three positions (x_s, x_h, x_r) move upstream again, this time showing a higher L_I/L_{II} ratio. At the end of the process ($t > 18$ s), the bubble stabilizes in the same positions of the case bubble without forcing.

The separation angle (α) evolution was evaluated in Fig. 15a. The average behavior seems to vary linearly until approximately $t = 16$ s. This parameter is less sensitive to changes in L_I and L_{II} lengths and maintains an approximately linear growth trend along the transient. Only when the bubble assumes the quasi-stationary topology does it stop growing. Regarding the behavior of the bubble height, we also observe a growth until close to $t = 16$ s (Fig. 15b). It is interesting to mention that the maximum bubble height is reached only after its maximum elongation. As well as α , h presented final values coinciding with those obtained for the bubble in the case without disturbance.

Information about the formation and ejection of the vortical structures was extracted by applying the λ_2 criterion. In Fig. 16, the formation of a vortex intensity in the region near the maximum bubble height can be seen, at time instants close to those of maximum bubble elongation. The vortex intensity grows as the bubble expands and does not seem to cause a noticeable bubble size reduction (Fig. 16a,

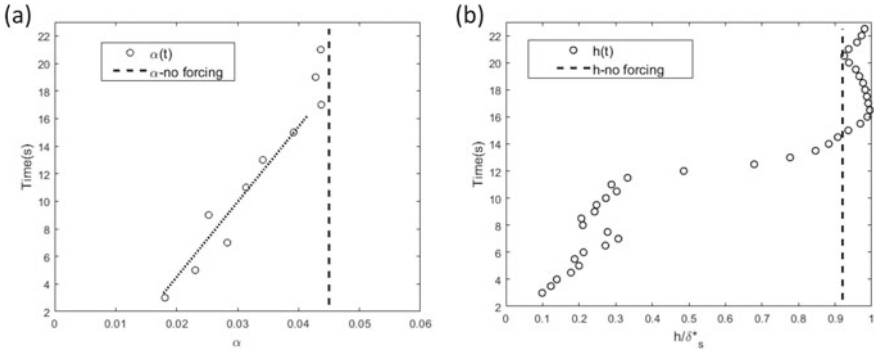


Fig. 15 **a** Separation angle and **b** bubble height evolution during the bubble growth. Circle: experimental data, dashed line: no forcing case

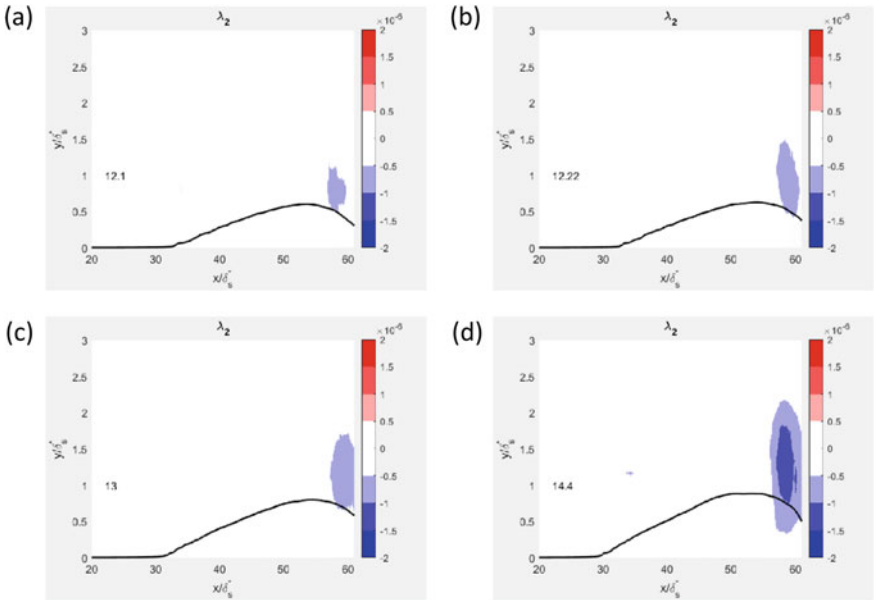


Fig. 16 λ_2 contour for some instants at the transient regime during the maximum bubble expansion. Solid line: streamline $\psi = 0$

b, respectively). With the presence of the most elongated bubble the vortex slightly changes its core position and grows in intensity (Fig. 16c, d). The stronger vortex causes a greater mixture between the separated and the non-separated fluid. From this instant on the separation bubble starts to reduce its size. Besides acting on the bubble length, the presence of a large energy vortex excites the formation of a small vortex further upstream and a periodic vortex shedding starts. According to Fig. 17, the bubble shortening ceases around $t = 18$ s. In the quasi-stationary regime, a fusion

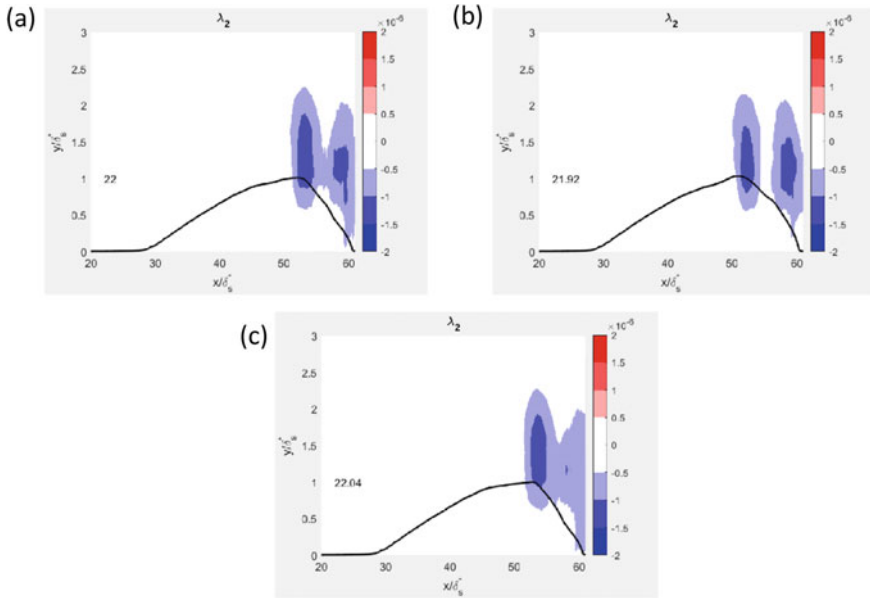


Fig. 17 λ_2 for the final stages of the transient process. Solid line: streamline $\psi = 0$

between pair of vortices subsequently formed is also observed (Fig. 17a–c). These results suggest that this small change in the interaction between the bubble and the vortex ejection is capable of promoting significant changes in the phenomenon topology. This process may be associated with the phenomenon of bubble flapping or even bursting.

9.4 Conclusion

This work aimed at studying the behavior of a laminar separation bubble subjected to a sudden variation in the level of flow disturbances. Despite the practical relevance for turbines, wind generators, and UAVs, the problem was little addressed in the literature. The study was conducted in a low turbulence water channel. The pressure gradient required for the separation bubble formation was obtained with a convergent–divergent plate. Before the disturbance system installation, flow velocity fields were measured with the presence of a trip close to the leading edge of the flat plate and, consequently, without the presence of the bubble. The objective was to characterize the pressure gradient imposed on the flow with the convergent–divergent plate. At the second moment, without the presence of the trip, the separation bubble phenomenon was measured and validated by comparison with the results presented in the literature. A vibrating ribbon was used to introduce controlled disturbances in

the flow and promotes the bubble elimination. After the bubble vanishes, the disturbance was turned off and the transient bubble recovery was measured using the PIV technique, with high temporal resolution. In this transient process, between the time when the flow is not separated and the moment when the bubble exhibits quasi-steady state, some topological parameters was analyzed, such as velocity contours; velocity profile at the separation point; separation point positions, reattachment, and maximum bubble height; separation angle; bubble height; and Re_{0s} .

According to the results, the momentum thickness Reynolds number and the shape factor at the separation point showed practically invariances in the transient regime. This differs from the results obtained for other parameters, such as the separation and reattachment points, the size and height of the bubble, and the separation angle. This behavior indicates that the boundary layer separation, in fact, is not much influenced by downstream flow dynamics. This result is interesting and unprecedented in the literature. Another interesting result was the analysis of the bubble topology during the transient. It was observed that there is little variation in the dimensionless form of the bubble. Significant differences in bubble shape were noted only in the instants very close to the beginning of the process. This suggests that in the case studied, the mechanism governing the shape of the separation bubble does not change significantly during the transient. Under the conditions of this study the bubble is close to the bursting, according to Gaster's criteria (1966). Indeed, in the undisturbed experiments, bubble reattachment oscillation was observed around a medium position. Under the transient regime, the bubble elongated to a greater length than that observed in the undisturbed case. Only after the ejection of the first high-intensity vortex the bubble reduced its size and moved to oscillate around the quasi-steady length. The association of the bubble length with vortex ejection had been reported in the work of Michelis et al. (2017). This behavior could be verified in detail due to the high temporal resolution in the measurement of the velocity fields.

After the transitional period, the bubble recovered completely the quasi-steady state. The recovery time was of the order of 20 s. This value is only an estimate, due to a discontinuity observed in the time series of the velocity fields. This discontinuity is probably associated with the data capture in two different moments. Although the problem has hindered the analysis of the temporal evolution of some bubble parameters, it does not compromise the observations and conclusions of the work. The results obtained contribute to characterize the complex dynamics of the transient regime of separation bubbles, providing new information about the phenomenon and supporting the development of tools for modeling the problem.

References

- Akpolat T et al (2012) Low Reynolds number flows and transition. *Low Reynolds Number Aerodynamics and Transition*, Mustafa Serdar Genc, IntechOpen. <https://doi.org/10.5772/31131>
- Diwan SS, Ramesh ON (2009) On the origin of the inflectional instability of a laminar separation bubble. *J Fluid Mech* 629:263–298

- Dovgal A, Kozlov V, Michalke A (1994) Laminar boundary layer separation: instability and associated phenomena. *Progr Aerosp Sci*, Elsevier 30(1):61–94
- Gaster M (1966) The structure and behavior of laminar separation bubbles. In: AGARD CP-4, pp 813–854
- Gaster M (1969) The structure and behavior of laminar separation bubbles. Rep. Mem. No. 3595. Aeronautical Research Council
- Hain R, Kahler C, Radespiel R (2009) Dynamics of laminar separation bubbles at low-reynolds-number aerofoils. *J Fluid Mech*, Cambridge University Press 630:129–153
- Hatman A, Wang T (1998) Separated-flow transition. Part 2 – Experimental results. *ASME Turbo Expo (98-GT- 462)*
- Lengani D et al (2017) Experimental investigation on the time–space evolution of a laminar separation bubble by proper orthogonal decomposition and dynamic mode decomposition. *J Turbomach, Am Soc Mech Eng Digital Collect* 139(3)
- Mayle RE (1991) The role of laminar-turbulent transition in gas turbine. *ASME J Turbomach* 113:509–537
- Marxen O, Henningson DS (2011) The effect of small-amplitude convective disturbances on the size and bursting of a laminar separation bubble. *J Fluid Mech*, Cambridge University Press 671:1–33
- Michelis T, Yarusevych S, Kotsonis M (2017) Response of a laminar separation bubble to impulsive forcing. *J Fluid Mech*, Cambridge University Press 820:633–666
- Pinedo OEO (2018) Projeto e Qualificação de um Aparato para o Estudo Experimental de Bolhas de Separação Laminar. Master Thesis, PUC-Rio
- Rodríguez D, Gennaro EM, Juniper MP (2013) The two classes of primary modal instability in laminar separation bubbles. *J Fluid Mech*. Cambridge University Press 734
- Serna J, Lázaro B (2015a) On the bursting condition for transitional separation bubbles. *Aerosp Sci Technol*, Elsevier 44:43–50
- Serna J, Lázaro BJ (2015b) On the laminar region and initial stages of transition in transitional separation bubble. *Eur J Mech B/Fluids* 49:171–183
- Swift K (2009) An experimental analysis of the laminar separation bubble at low Reynolds numbers. Master Thesis, University of Tennessee –Knoxville, Tennessee, EUA
- Tani I (1964) Low speed flows involving separation bubbles. *Prog Aeronaut Sci* 5:70–103
- Yarusevych S, Kotsonis M (2017) Steady and transient response of a laminar separation bubble to controlled disturbances. *J Fluid Mech* 813:955–990